Nanoscale Advances

ROYAL SOCIETY OF CHEMISTRY

PAPER

View Article Online
View Journal | View Issue

Cite this: *Nanoscale Adv.*, 2021, **3**, 2617

A SERS-active capillary for direct molecular trace detection in liquids

Zhoutao Sun, Chen Kang, Xiaohui Fang, * Hongmei Liu, Jinxin Guo and Xinping Zhang *

Received 3rd February 2021
Accepted 7th March 2021

DOI: 10.1039/d1na00082a

rsc.li/nanoscale-advances

The development of Surface Enhanced Raman Scattering (SERS) promotes the wide application of Raman spectroscopy in chemical and biomolecular detection. SERS detection relies on analytes in close contact with the metallic surface, and therefore direct molecular trace detection in the liquid phase is difficult. In this paper, static liquid phase SERS detection was performed simply using a capillary without pre-functionalization. Gold nanoparticles (AuNPs) with an optimized size ensure localized surface plasmons in resonance with the exciting laser light. Grazing incidence and multimode interference in the capillary ensure that the longitudinal Raman signal is effectively excited and accumulated. An enhancement factor as high as 10^8 and a detection limit of 10^{-9} M of crystal violet in aqueous solution have been achieved.

Introduction

SERS is widely used in environmental protection, food safety, and other fields because of its high sensitivity and extremely low detection concentration.[1–5] Traditionally, SERS detection is performed on a planar SERS-active surface, and Raman scattering enhancement relies on analytes in solution to diffuse sufficiently close to the SERS-active sites. The detection of analytes with low concentrations is challenging due to a small number of analytes in close contact with the metallic surface. To promote sensitivity, two main approaches were employed. One is preconcentration of analyte molecules through drying[6] or chemical affinity.[7] The enhancement factor can reach as high as 10^{10} to 10^{14}.[8–10] However, preconcentration is time-consuming and unfavourable for static liquid or gas phase detection. The other one is to lengthen the working distance and effectively collect Raman scattering. Therefore, 3-D SERS detection was proposed and developed.[11] A photonic crystal fiber (PCF) allows direct incorporation of analytes into axially aligned air channels; the interaction between the analyte and excitation light could be increased many fold. Moreover, a PCF can guide both excitation and Raman signals. It can simultaneously function as an excitation and collection platform. Therefore, SERS-active PCF probes provide a unique opportunity to develop optofluidic liquid sensors with high sensitivity.[12] The numerous PCF designs can be classified into two main categories. One is a solid-core PCF, which always has a core size of less than 5 μm and needs fine tuning for laser coupling. The other one is a hollow-core PCF. It requires selectively filling the liquid-analyte into the air channels to avoid bandgap properties which is also complicated. In addition, in previous studies, SERS-active metallic nanoparticles were always decorated on microchannels. This is suitable and necessary for *in situ* needle sensors, but the functionalization procedure along the microchannels of several centimeters long is complicated. In most situations, such as water environment and food safety testing, *in situ* detection is not necessary and it is feasible to premix SERS-active nanoparticles with the analyte which is much simpler and easier than the functionalization procedure.

In this paper, we report a simple and effective SERS-active capillary scheme. Similar to PCFs, the capillary samples and analyzes the test solution simply using capillary force, and the excitation light and Raman-scattered photons can propagate along the entire length which greatly increases the number of SERS-active sites.[13] Moreover, capillaries have only one large air channel which means it is easy for fabrication and light coupling. Leaky modes in the hollow core interfere with each other forming an enhanced field distribution. Spherical AuNPs were synthesized by reducing chloroauric acid ($HAuCl_4$) using sodium citrate (SC). The analyte is premixed with the AuNPs to form the SERS-active solution. By adjusting the particle size of AuNPs, the localized surface plasmons become in resonance with the exciting laser light. In order to characterize the practicality of this method, we tested the content of crystal violet (CV) in aqueous solution. CV can effectively kill fungi and parasitic infections in fish, and has been widely used in aquaculture. However, it was discovered that CV has carcinogenic and teratogenic side effects. In recent years, it has been strictly prohibited to be used in aquatic products. Therefore, it is of practical significance to detect the CV content in aqueous solution. A detection limit of 10^{-9} M and an enhancement factor (EF) as high as 10^8 have been achieved.

Institute of Information Photonics Technology and Faculty of Science, Beijing University of Technology, Beijing 100124, China. E-mail: fangxh@bjut.edu.cn; zhangxinping@bjut.edu.cn

Experimental

Chemicals and materials

$HAuCl_4$ and CV were purchased from Sinopharm Chemical Reagent Co., Ltd. SC was purchased from Aladdin. Sodium chloride (NaCl) was purchased from Beijing Chemical Works. The quartz capillary tube (inner diameter of 40 μm) was purchased from INNOSEP. Milli-Q deionized water was used in all the experiments.

Synthesis and characterization of gold nanoparticles

AuNPs were synthesized by reducing $HAuCl_4$ with SC.[14–16] On the basis of seed solution, AuNPs with different particle sizes were grown by generation. The first step involved the preparation of the seed solution. A solution of 2.2 mM SC solution in Milli-Q water (150 mL) was stirred and heated to boiling, and then 1 mL of $HAuCl_4$ (25 mM) was added. During the process, the color of the solution changes from yellow to light pink, and finally to wine red, which means that the preparation of the seed solution was completed. After the gold seeds were synthesized, the temperature of the seed solution was quickly decreased and kept at 90 °C. $HAuCl_4$ (25 mM, 1 mL) was added twice with an interval time of 30 min. At this point, the first generation of AuNPs was achieved. 55 mL of the first-generation solution was extracted and mixed with 53 mL of Milli-Q water and 2 mL of SC (60 mM). This solution was then used as a seed solution for the synthesis of the next generation of AuNPs. The above process was repeated until the seventh generation, and AuNPs with sizes ranging from 20 to 110 nm were obtained.

The TEM images of AuNPs were obtained by high-resolution transmission electron microscopy (HRTEM). The absorption spectra of each generation of AuNPs were obtained by UV-vis spectroscopy.

SERS measurements

Aqueous solutions of CV with concentrations from 10^{-5} M to 10^{-10} M were prepared by mixing the CV solutions of 10^{-4} M to 10^{-9} M with gold nanoparticles at a 1 : 9 ratio in volume. The tip of the quartz capillary tube was immersed into the mixed SERS-active solution for 2 min. Then, the SERS spectra were measured using a confocal Raman spectroscopy system (WITec), using lasers with emission wavelengths of 532 nm and 633 nm. A 50× objective lens (NA = 0.80, Olympus) coupled the laser light into the capillary core and collected the emitted Raman signal in backscattering configuration. A simplified schematic of this configuration is represented in Fig. 1(c). The integration time of each spectrum was set to 5 seconds, and the number of integrations was 1.

Results and discussion

Resonance characteristics of the SERS-active capillaries

The TEM images of AuNPs with different generations (G_1–G_7) are shown in Fig. 1(a). With the increase of synthetic generation, the diameter of the AuNPs gradually increases. And for each generation, the shape and size of the AuNPs are uniform.

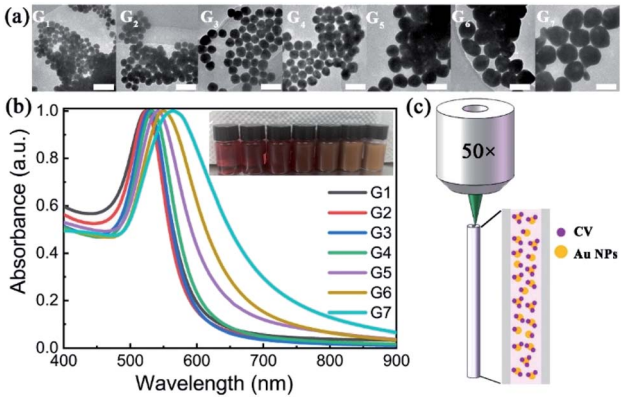

Fig. 1 (a) TEM images of different generations of AuNPs. Scale bar: 100 nm. (b) UV-vis absorption spectra of different generations of AuNPs. Inset: the photo of Au-NP aqueous solutions with different generations, from left to right corresponding to the first to the seventh generation. (c) Backscattering configuration of the capillary for Raman signal collection.

Corresponding to the generation from G_1 to G_7, the average sizes of the AuNPs are 30 nm, 36 nm, 44 nm, 54 nm, 68 nm, 86 nm, and 103 nm, respectively. The absorption spectra (UV-vis) of AuNP aqueous solutions with different generations (G_1–G_7) are shown in Fig. 1(b). With the increase of particle size, the absorption peak gradually red-shifted and the color of the solution gradually darkened. Corresponding to the generations from G_1 to G_7, the absorption peaks are centered at 524 nm, 525 nm, 528 nm, 533 nm, 542 nm, 550 nm, and 564 nm, respectively.

To characterize the Raman enhancement dependence on the AuNPs size, we measured the SERS spectra of 10^{-5} M CV solution with AuNP generations from G_1 to G_7, respectively. The excitation wavelength was 532 nm. The results are shown by solid lines in Fig. 2. The characteristic peaks of the CV SERS spectrum are mainly located at 916 cm^{-1}, 1173 cm^{-1}, 1585 cm^{-1}, and 1616 cm^{-1}, which are associated with the shear

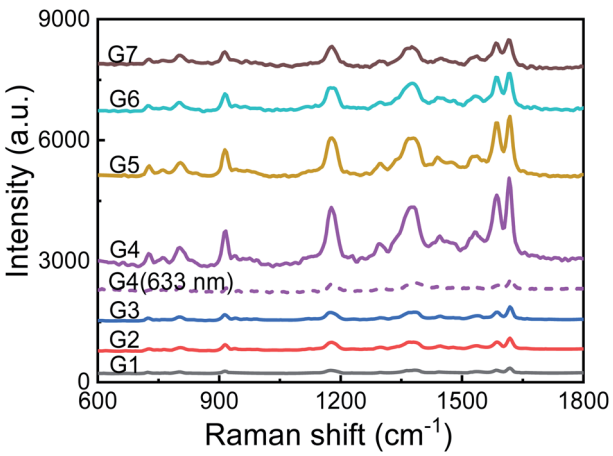

Fig. 2 Raman spectra of CV (10^{-5} M) with different sizes of AuNPs as SERS enhancing solution. Solid lines: excited by 532 nm laser light; purple dotted line: excited by 633 nm laser light.

vibration of the C–C–C bond, the in-plane rocking vibration of the C–H bond, and stretching vibrations of the C–C and C–N bonds, respectively. SERS is strongest with the use of the fourth generation of AuNPs. This is because the localized surface plasmon resonance wavelength of the fourth generation of AuNPs is 533 nm, which is the closest to the laser emission wavelength (532 nm). The electromagnetic field is greatly enhanced near the surface of the AuNPs, showing the strongest Raman signal compared to the other generations. Additionally, the optical scattering cross-section is also an important factor. AuNPs with a larger cross section (*e.g.* G_7) scatter a more intense Raman signal compared to the AuNPs with a smaller size (G_1–G_3), although the absorption peak of G_7 deviates more from the resonance wavelength. Therefore, we use the fourth-generation AuNPs for the following SERS detection.

To further demonstrate the resonance characteristics, we changed the wavelength of the excitation laser light to 633 nm. The Raman spectrum of 10^{-5} M CV solution premixed with the fourth generation of AuNPs is shown in Fig. 2 with the purple dotted line. The Raman signal is 40 times weaker at the peak of 1616 cm^{-1} compared to the signal when a 532 nm laser is used. The excitation laser in resonance with the localized surface plasmons of AuNPs significantly enhances the Raman signal.

Evaluation of the enhancement ability of the SERS-active capillary platform

To investigate the capability of the SERS-active capillary platform, we measured a series of low concentrations of CV solutions from 10^{-5} M to 10^{-9} M. The results are shown in Fig. 3(a). The detection limit is as low as 10^{-9} M. In order to further improve the detection sensitivity, NaCl saturated solution was added into the SERS-active solution. We mixed the CV solutions with AuNPs and NaCl solution at a 1 : 7 : 2 ratio in volume. For the CV concentrations of 10^{-10} M, the SERS peaks were still obvious (yellow line in Fig. 3(a), with 10 times magnification). This is because the presence of Cl^- can make AuNPs quickly aggregate and form stronger hot spots, thereby improving SERS sensitivity. Therefore, in order to detect a low concentration of the test solution, adding an appropriate amount of NaCl solution to the SERS-active solution is a simple and effective method.

In order to facilitate the understanding of the ultralow concentration of 10^{-10} M, we quantitatively calculate the number of AuNPs and CV molecules. The effective length of the capillary is measured by the cut-back technique. The detectable Raman scattering intensity remains unchanged with a capillary length range from 5 mm to 5 cm. Therefore, the effective volume of the SERS-active solution is less than 6.28 nL. According to the synthesis procedure, the concentration of the fourth generation of AuNPs is 4.8×10^{11} NPs per mL.[14] The number of AuNPs and CV molecules is 2.7×10^6 and 3.78×10^5, respectively. This means that for one sample molecule, 71 AuNPs may interact with it. For static liquid detection, the sample molecules are evenly dispersed in the solution while the AuNPs are aggregated because of the addition of Cl^-. Therefore, the ratio of AuNPs and CV molecules should be much greater than 71. From this perspective, it can be considered that the experimentally measured SERS spectra are derived from a very small number of sample molecules.

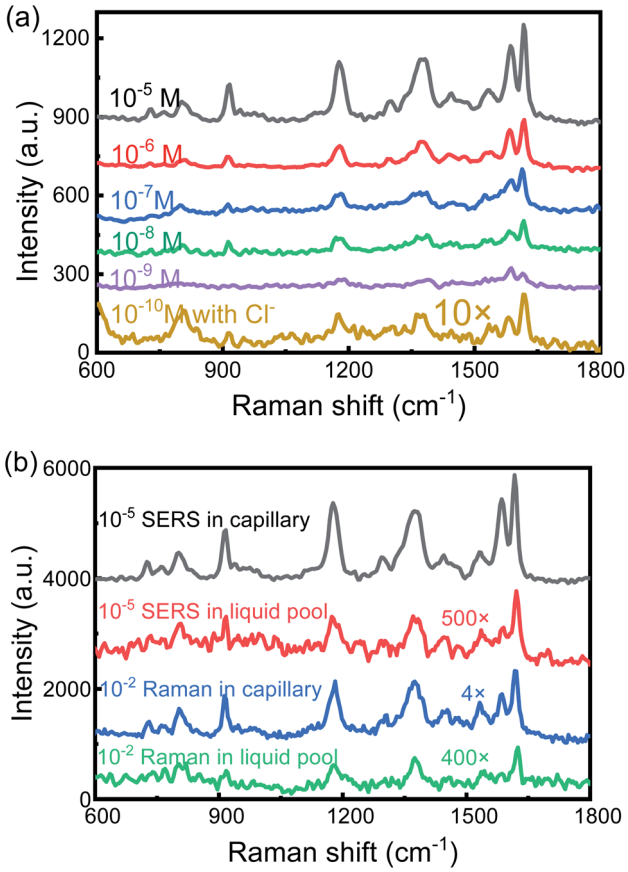

Fig. 3 (a) SERS spectra of CV with concentrations from 10^{-5} M to 10^{-10} M. Cl^- is added into 10^{-10} M CV solution for AuNP aggregation forming more SERS-active spots. The spectrum intensity with a concentration of 10^{-10} M is 10 times magnified. (b) SERS spectra of 10^{-5} M CV aqueous solution mixed with AuNPs in the capillary (black line) and in the liquid pool (red line, with 500 times magnification). Normal Raman spectrum of 10^{-2} M CV in the capillary (blue line, with 4 times magnification) and in the liquid pool (green line, with 400 times magnification).

To evaluate the Raman enhancement ability based on the SERS-active capillary, the normal Raman scattering spectrum of CV solution in the liquid pool is also measured. The detection limit of CV without AuNPs is only 10^{-2} M. For comparison, the SERS spectrum of 10^{-5} M CV in the liquid pool and normal Raman spectrum of 10^{-2} M CV in the capillary were also measured. The results are shown in Fig. 3(b). The EF of the Raman signal is calculated according to eqn (1):[17]

$$EF = \left(\frac{I_{SERS}}{I_{Bulk}}\right)\left(\frac{C_{Bulk}}{C_{SERS}}\right) \quad (1)$$

C_{SERS} and C_{Bulk} are the concentrations of CV solution that can be detected with and without AuNPs, which are 10^{-9} M and 10^{-2} M, respectively. I_{SERS} and I_{Bulk} are the measured SERS and normal Raman scattering intensities, respectively. We used the strongest signature stretching modes at 1616 cm^{-1}, which are

21 and 1.5, respectively. The calculated EF value of our SERS-active capillaries is 1.4×10^8. The enhancement is mainly attributed to the localized surface plasmon resonance of AuNPs. Additional enhancement results from the use of a capillary. The capillary provides a larger surface area in the focus volume and also collects and accumulates longitudinal Raman scattering which greatly enhances the detectable Raman intensity. In a comparison of the SERS spectra in the capillary and in the liquid pool, the peak intensity at 1616 cm^{-1} was found to be 500 times enhanced by using the capillary (Fig. 3(b)).

When PCFs are used as SERS needle sensors, the excitation laser light needs to be carefully coupled into the core and the accumulated back-scattered Raman signal is also mainly distributed in the fiber core.[19] Different from PCFs, the capillary has a low intensity Raman signal in the liquid channel center. Fig. 5(a) shows the hyperspectral Raman image of CV (10^{-5} M SERS-active mixed solution) at 1616 cm^{-1}. The measurement process is shown in the inset; the sample is scanned in the x and y directions stepwise with a step size of 1.6 μm. The objective lens not only focuses the exciting laser beam, but also collects the returned Raman scattering. The Raman signal around the inner wall of the capillary is very strong and the thickness reaches 6 μm. This greatly reduces the difficulty of coupling adjustment. In addition, the relative standard deviation (RSD) of Raman intensities was calculated to evaluate the reproducibility of the SERS-active capillary. We detected the Raman signal of 10^{-5} M CV using five individual SERS-active capillaries. For each capillary, we randomly chose 6 different points within 6 μm from the capillary wall. The Raman spectra are shown in Fig. 4(a). As can be seen from this figure, all the spectral shapes match very well, and the characteristic peaks do not change. The RSD values of the 1173, 1585 and 1616 cm^{-1} peaks shown in Fig. 4(b) were calculated according to eqn (2):[18]

$$\mathrm{RSD} = \frac{\sqrt{\sum_{i=1}^{n}\left(I_i - \bar{I}\right)^2}}{\bar{I}} \quad (2)$$

where $n = 30$ is the number of Raman spectra, I_i is the Raman signal intensity of each characteristic peak, and $\bar{I}$ is the average intensity of Raman signal intensity. The variation of RSD values for 10^{-5} M CV was all within 15%, which indicated that the SERS-active capillary had good reproducibility.

To understand the Raman enhancement ability based on the SERS-active capillary, the hollow core capillary filled with water was simulated. As shown in Fig. 5(b), the reflectivity of the interface between water ($n_1 = 1.33$) and fused silica ($n_2 = 1.45$) varies with the angle of incidence. Most of the laser light transmits through fused silica and is lost when the incident angle is less than 60°, while the laser light is totally reflected when the incidence angle approaches 90°. Therefore, when the laser is incident near the inner wall of the capillary (Fig. 5(e)), the focused laser beam is highly reflected before diverging. The laser light can travel a long distance while keeping high intensity. In contrast, when the laser is incident to the liquid pool (Fig. 5(c)), the laser beam focus quickly expands and the intensity reduces to less than 30% with a propagation length

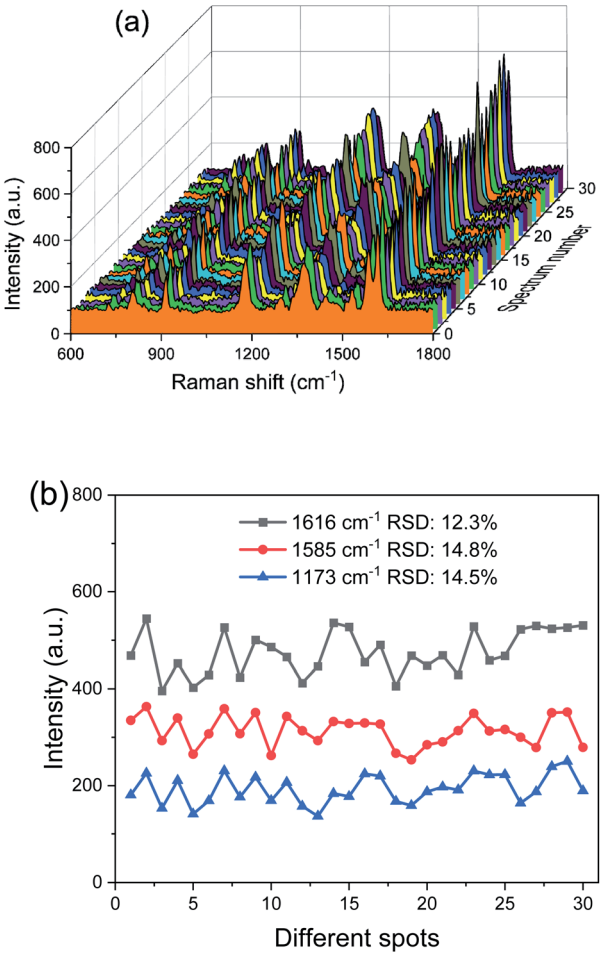

Fig. 4 (a) Raman spectra of 10^{-5} M CV at 30 different points obtained from five SERS-active capillaries. (b) the peak intensities of Raman bands at 1173, 1585 and 1616 cm^{-1} and the corresponding RSD values.

less than 0.4 mm. As the diameter of the capillary (40 μm) is much larger than the size of the focused laser beam (~2 μm), the focus of the laser beam incident on the center of the capillary (Fig. 5(d)) already expands and becomes too large before it reaches the fused silica, and there is not a strong enough intensity to generate detectable Raman signals. In addition, different from the liquid pool, the multimode interference in the capillary further extends the effective working distance. As shown in Fig. 5(f), the capillary has several leaky modes. The focused laser beam coupled into the capillary excites several modes. The multimode interference forms an enhanced field distribution along the capillary length (Fig. 5(d) and (e)). According to the coupled mode theory, the off-center injection excites only non-centrosymmetric high-order modes. Therefore, it forms a more concentrated field distribution along the capillary length and excites stronger Raman scattering. Overall, although the channel size of the capillary is large, the laser light is not evenly distributed in the liquid core; the enhanced field distribution and the long propagation length make the SERS-active capillary suitable for static liquid detection.

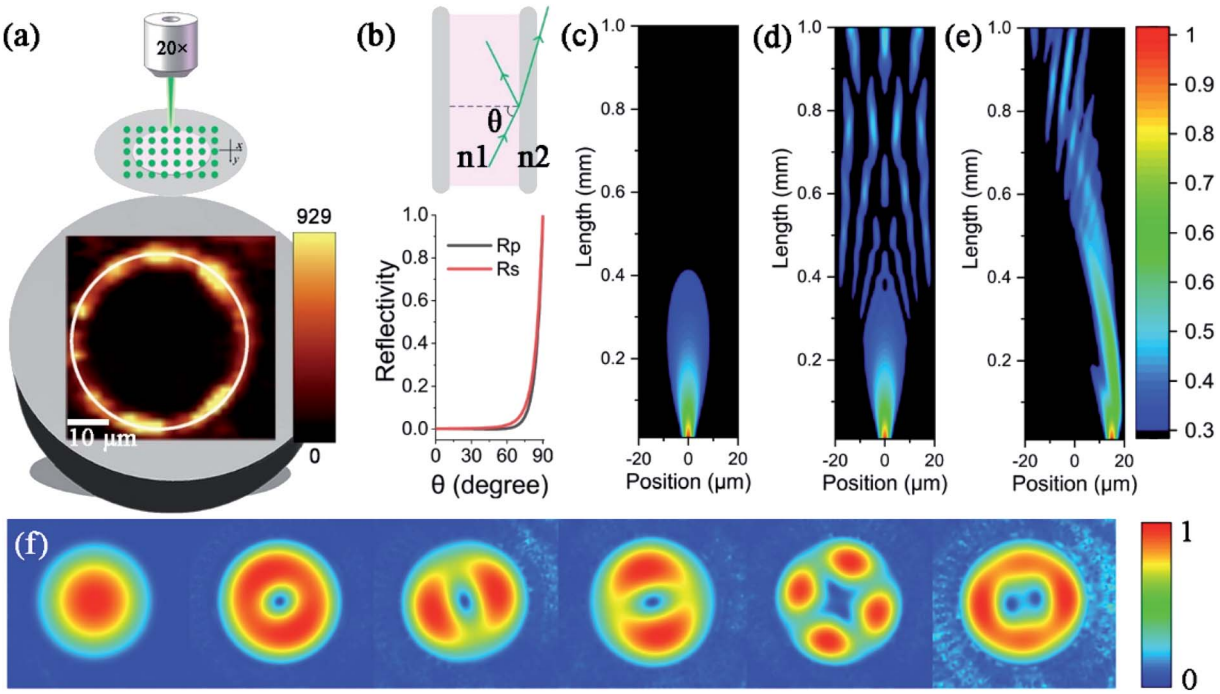

Fig. 5 (a) Raman map of the end face of the capillary filled with CV (10^{-5} M SERS-active mixed solution) obtained at 1616 cm^{-1}. The mapping area is 50 μm × 50 μm under a 20× objective lens. A white circle is added to indicate the inner wall of the capillary; inset: schematic diagram of the mapping process; (b) the incident angle dependence of the reflectivity of p-polarized (R_p) and s-polarized (R_s) light at the interface of water ($n_1 = 1.33$) and fused silica ($n_2 = 1.45$); the propagation properties of the focused laser light in the liquid pool (c) and in the water filled capillary with the injection position at the core center (d) and near the inner wall (e); (f) the leaky mode distribution of the capillary filled with water.

Conclusions

In summary, we have developed a platform for sensitive SERS detection using a capillary. The capillary samples and analyses premixed SERS-active solution simply using capillary force. Raman scattering is enhanced by three main mechanisms. The first and the most important one is the optimization of the AuNP size which ensures the localized surface plasmons are in resonance with the exciting laser light. The second one is that when the excitation laser is incident near the inner wall of the capillary, the high-intensity and long-distance propagation allows the longitudinal Raman signal to be effectively excited and accumulated. The third one is the multimode interference in the capillary which further extends the effective working length. Ultrasensitive detection with an EF as high as 10^8 and a detection limit of 10^{-9} M for CV in aqueous solution has been achieved. The sensitivity can be further improved by optimizing the multimode interference distribution through adjusting the air channel diameter and the length of the capillary. It is worth noting that the EF is obtained by detecting the test solution directly in the static liquid phase without pretreatment of the capillary and the preconcentration of the test solution. The simple, cost effective fabrication and low sample consumption are suitable for rapid detection in various practical applications.

Conflicts of interest

There are no conflicts to declare.

Acknowledgements

We acknowledge the National Natural Science Foundation of China (61575007) for the financial support.

Notes and references

1 D. W. Li, W. L. Zhai, Y. T. Li and Y. T. Long, *Microchim. Acta*, 2014, **181**, 23–43.
2 Y. K. Gao, N. Yang, T. T. You, C. M. Zhang and P. G. Yin, *Sens. Actuators, B*, 2018, **267**, 129–135.
3 J. Y. Fei, L. Wu, Y. Z. Zhang, S. F. Zong, Z. Y. Wang and Y. P. Cui, *ACS Sens.*, 2017, **2**, 773–780.
4 A. P. Craig, A. S. Franca and J. Irudayaraj, in *Annual Review of Food Science and Technology, Vol 4*, ed. M. P. Doyle and T. R. Klaenhammer, Annual Reviews, Palo Alto, 2013, vol. 4, pp. 369–380.
5 X. M. Kong, X. Y. Chong, K. Squire and A. X. Wang, *Sens. Actuators, B*, 2018, **259**, 587–595.
6 R. L. Aggarwal, L. W. Farrar and S. K. Saikin, *J. Phys. Chem. C*, 2012, **116**, 16656–16659.
7 Y. Shin, I. Jeon, Y. You, G. Song, T. K. Lee, J. Oh, C. Son, D. Baek, D. Kim, H. Cho, H. Hwang, T. Kim, S. K. Kwak, J. Kim and J. Lee, *Adv. Opt. Mater.*, 2020, **8**, 10.
8 K. A. Willets and R. P. Van Duyne, *Annu. Rev. Phys. Chem.*, 2007, **58**, 267–297.
9 G. K. Pandey, N. K. Pathak, A. Ji, H. Pathak and R. P. Sharma, *Plasmonics*, 2016, **11**, 1343–1349.

10 J. Song, J. H. Xian, M. H. Yu, D. Wang, S. Ye, H. B. Niu, X. Peng and J. L. Qu, *IEEE Photonics J.*, 2015, **7**, 8.
11 W. Xie, B. Walkenfort and S. Schlucker, *J. Am. Chem. Soc.*, 2013, **135**, 1657–1660.
12 Y. Han, S. L. Tan, M. K. K. Oo, D. Pristinski, S. Sukhishvili and H. Du, *Adv. Mater.*, 2010, **22**, 2647–2651.
13 S. Yuksel, A. M. Schwenke, G. Soliveri, S. Ardizzone, K. Weber, D. Cialla-May, S. Hoeppener, U. S. Schubert and J. Popp, *Anal. Chim. Acta*, 2016, **939**, 93–100.
14 N. G. Bastus, J. Comenge and V. Puntes, *Langmuir*, 2011, **27**, 11098–11105.
15 Y. G. Sun and Y. N. Xia, *Science*, 2002, **298**, 2176–2179.
16 S. Eustis and M. A. El-Sayed, *Chem. Soc. Rev.*, 2006, **35**, 209–217.
17 M. Shanthil, H. Fathima and K. George Thomas, *ACS Appl. Mater. Interfaces*, 2017, **9**, 19470–19477.
18 H. M. Parsons, D. R. Ekman, T. W. Collette and M. R. Viant, *Analyst*, 2009, **134**, 478–485.
19 M. K. K. Oo, Y. Han, J. Kanka, S. Sukhishvili and H. Du, *Opt. Lett.*, 2010, **35**, 466–468.